Negligible Surface Reactivity of Topological Insulators Bi_2Se_3 and Bi_2Te_3 towards Oxygen and Water

Lada V. Yashina,[†,▽,*] Jaime Sánchez-Barriga,[‡,▽] Markus R. Scholz,[‡,▽] Andrey A. Volykhov,[†,§,▽] Anna P. Sirotina,[†,▽] Vera, S. Neudachina,[†,⊥,▽] Marina E. Tamm,[†,▽] Andrei Varykhalov,[‡,▽] Dmitry Marchenko,[‡,▽] Gunther Springholz,[∥,▽] Günther Bauer,[∥,▽] Axel Knop-Gericke,[#,▽] and Oliver Rader[‡,▽]

[†]Department of Chemistry, Moscow State University, Leninskie Gory 1/3, 119991 Moscow, Russia, [‡]Helmholtz-Zentrum Berlin für Materialien und Energie, Elektronenspeicherring BESSY II, Albert-Einstein-Strasse 15, 12489 Berlin, Germany, [§]Kurnakov Institute of General and Inorganic Chemistry RAS, Leninsky Av 31, 119991 Moscow, Russia, [⊥]Federal State Research and Design Institute of Rare Metal Industry (GIREDMET), 5 bldg. 1 B. Tolmachevskylane, 119017 Moscow, Russia, [∥]Institut für Halbleiter- und Festkörperphysik, Johannes Kepler Universität, Altenbergerstrasse 69, 4040 Linz, Austria, and [#]Fritz-Haber-Institut der Max-Planck-Gesellschaft, Faradayweg 4-6, 14195 Berlin, Germany. [▽]All authors contributed equally.

ABSTRACT The long-term stability of functional properties of topological insulator materials is crucial for the operation of future topological insulator based devices. Water and oxygen have been reported to be the main sources of surface deterioration by chemical reactions. In the present work, we investigate the behavior of the topological surface states on Bi_2X_3 (X = Se, Te) by valence-band and core level photoemission in a wide range of water and oxygen pressures both *in situ* (from 10^{-8} to 0.1 mbar) and *ex situ* (at 1 bar). We find that no chemical reactions occur in pure oxygen and in pure water. Water itself does not chemically react with both Bi_2Se_3 and Bi_2Te_3 surfaces and only leads to slight *p*-doping. In dry air, the oxidation of the Bi_2Te_3 surface occurs on the time scale of months, in the case of Bi_2Se_3 surface of cleaved crystal, not even on the time scale of years. The presence of water, however, promotes the oxidation in air, and we suggest the underlying reactions supported by density functional calculations. All in all, the surface reactivity is found to be negligible, which allows expanding the acceptable ranges of conditions for preparation, handling and operation of future Bi_2X_3-based devices.

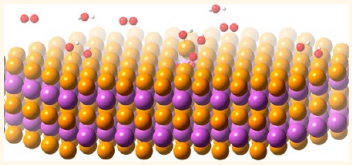

KEYWORDS: topological insulators · surface reactivity · topological surface states · angle-resolved photoemission · high-pressure XPS

The Bi_2Se_3 and Bi_2Te_3 compounds are referred to as the second generation of topological insulators.[1−8] Topological insulators exhibit a metallic surface and an insulating bulk where the bulk band gap is an inverted gap caused by a strong spin−orbit interaction. The metallic surface bands have a Dirac-like dispersion similar to graphene[9] but with a peculiar spin texture which is locked to the electron momentum.[10] These properties lead to interesting charge and spin transport phenomena such as the forbidden 180° backscattering.[11]

In contrast to graphene, the peculiar spin texture of the Dirac cone means a topological protection of the surface state by time-reversal symmetry.[5] In the case of Bi_2Se_3 and Bi_2Te_3, there is a single Dirac cone on each surface, for which the natural cleavage plane is easily accessible. The Dirac cone arises due to unequal topological invariants on each side of the surface, which means that it is robust towards external perturbations.[5−8] This includes surface reactions, at least at their initial stages, as it was demonstrated experimentally in several publications.[12−18] This protection apparently does not work in the case of a chemical reaction that converts the near surface region of a sample to a topologically trivial material, in which the protected surface state is expected to move to the buried interface. Before the latter can be proven, which is by itself challenging using surface sensitive spectroscopies such as angle-resolved photoelectron spectroscopy (ARPES), the question has to be answered whether and which chemical reaction takes place. The role of the topological protection for the surface reactivity is an aspect that has not been studied intensively so far.

Device applications do require detailed knowledge with regard to the stability limits of the surface properties and the behavior

* Address correspondence to yashina@inorg.chem.msu.ru.

Received for review February 22, 2013 and accepted May 16, 2013.

Published online May 16, 2013
10.1021/nn400908b

of the topological surface state under ambient conditions, especially as preparation techniques are being extended toward ultrathin freestanding layers, nanotubes, and patterning by lithography. Up to now only few studies on the surface reactivity of topological insulator materials have been performed, and the results reported are controversial.

Alongside with many chalcogenides (IV–VI, II–VI compounds), Bi_2Se_3 and Bi_2Te_3 are expected to undergo surface oxidation under ambient environment, however, they have a layered structure, which is typically associated with low reactivity, *e.g.*, in the case of GaSe and InSe.[19,20] The surface reactivity of layered compounds correlates with the strength of weak interlayer interaction, this being higher in the case of higher interaction, for instance for SnSe. Generally, tellurides tend to be more chemically reactive than selenides.[21]

The kinetics of the Bi_2Te_3 surface oxidation in air at 30% relative humidity was studied by Bando *et al.*[22] According to these data, a pronounced and relatively fast surface reaction occurs between 1 day and 7 days of air exposure, although the oxidation mechanism at the initial stage remains unclear.

The reactivity of the Bi_2Se_3 surface is a more complex issue. ARPES studies[23] demonstrated acceptor behavior of oxygen deposited at low temperature under ultrahigh vacuum (UHV) conditions by a shift of the topological surface state to lower binding energy. This is consistent with the assumption of molecular adsorption. Density functional theory (DFT) calculations[24] predict that molecular adsorption of O_2 should result in rather weak bonding (bond energy ~0.12 eV). The topological surface states of Bi_2Se_3 preserves. Contrary, a reaction with atomic oxygen removes the original surface state and yields two new surface states.

Prolonged exposure of Bi_2Se_3 to the residual gas in a UHV chamber leads to donor doping of the topological surface state.[16] The resulting band bending effect is so strong that a two-dimensional electron gas with a Rashba-type spin–orbit splitting appears.[16] Interestingly, the size of the Rashba splitting was reported to increase with time, *i.e.*, with the amount of the residual gas adsorbed. Similar effects have been obtained by controlled exposure to CO[16] and water.[14] According to ref 14, the donor doping of the topological surface state and the Rashba splitting effects observed in ARPES under relatively low water dosages (up to 700 L) at room temperature are related to the surface reaction; however, a direct proof, *e.g.*, by observation of systematic changes in the corresponding core level spectra, has not been provided. Rapid surface oxidation of Bi_2Se_3 at ambient environment and donor oxygen doping are reported in ref 25, indicating that oxygen is the main cause for the surface degradation of Bi_2Se_3.[25] Contrary to this, in refs 26 and 27, high stability of the cleaved Bi_2Se_3 crystal surfaces is stated.

In the present paper, we report a systematic and comprehensive ARPES and core level photoemission study for both Bi_2Se_3 and Bi_2Te_3 surfaces of cleaved Bridgman crystals as well as MBE grown epilayers of *n*-type conductivity in oxygen and/or water environments, including high-pressure XPS experiments.

RESULTS AND DISCUSSION

The air oxidation of bismuth chalcogenides proceeds in several steps, which are:

(i) Molecular adsorption and induction period;
(ii) Surface reaction and oxidation of the first layer;
(iii) In-depth oxidation with long-term kinetics.The following discussion is organized in accordance with these steps.

Molecular Adsorption of O_2 and H_2O on Bi_2Te_3 (111) and Bi_2Se_3 (111). The ARPES $E(\mathbf{k})$ dispersions for the O_2/Bi_2Te_3 system obtained at 30 K are illustrated in Figure 1a–f. It is evident that oxygen molecules cause acceptor doping of the topological surface state as expected *a priori* like it was observed for many semiconductor surfaces. The dosage dependence presented in Figure 1g shows that the Fermi level decreases by 0.26 eV. In other words, the Dirac point is upshifted from 0.36 to 0.08 eV binding energy. Similar doping behavior was observed previously for Bi_2Se_3.[23] Despite this strong doping effect of oxygen, we do not observe any changes in the spectral shapes of the Bi 5f and Te 4d core levels. Bi 5d core level is shown in Figure 1h. Therefore, oxygen adsorbs molecularly. Almost reversible adsorption is confirmed by the corresponding shift away from the Fermi level during subsequent sample heating (Figure 1f).

According to our DFT modeling results, the most stable position of the oxygen molecules at the surface is different from the on-top geometry previously proposed for Bi_2Se_3,[24] where the O–O bonds are perpendicular to the surface. As shown in Figure 1i, in our optimized structure the O–O bond is almost parallel to the surface. For this geometry, the position of the Fermi level is lower than for the clean surface by ~0.21 eV (for the coverage of one O atom per 1 surface Te atom). In other words, the acceptor doping behavior of molecular oxygen is also confirmed by our calculations. We obtained similar theoretical results for the Bi_2Se_3 surface (see Table 1).

The sequence of energy-momentum dispersions obtained for Bi_2Se_3 and Bi_2Te_3 during water adsorption up to 500 L exposure at room temperature is shown in Figures 2a–d and 3a–d, respectively. A very weak acceptor doping of the topological surface state is clearly observed. Moreover, as shown in Figures 2f–g and 3f–g, there are no systematic changes in the spectral shape of the corresponding Bi 5d and Te 4d/Se 3d core levels, *i.e.*, broadening and appearance of new components. This means that the formation of chemical bonds between the adsorbate and the surface proposed in ref 14

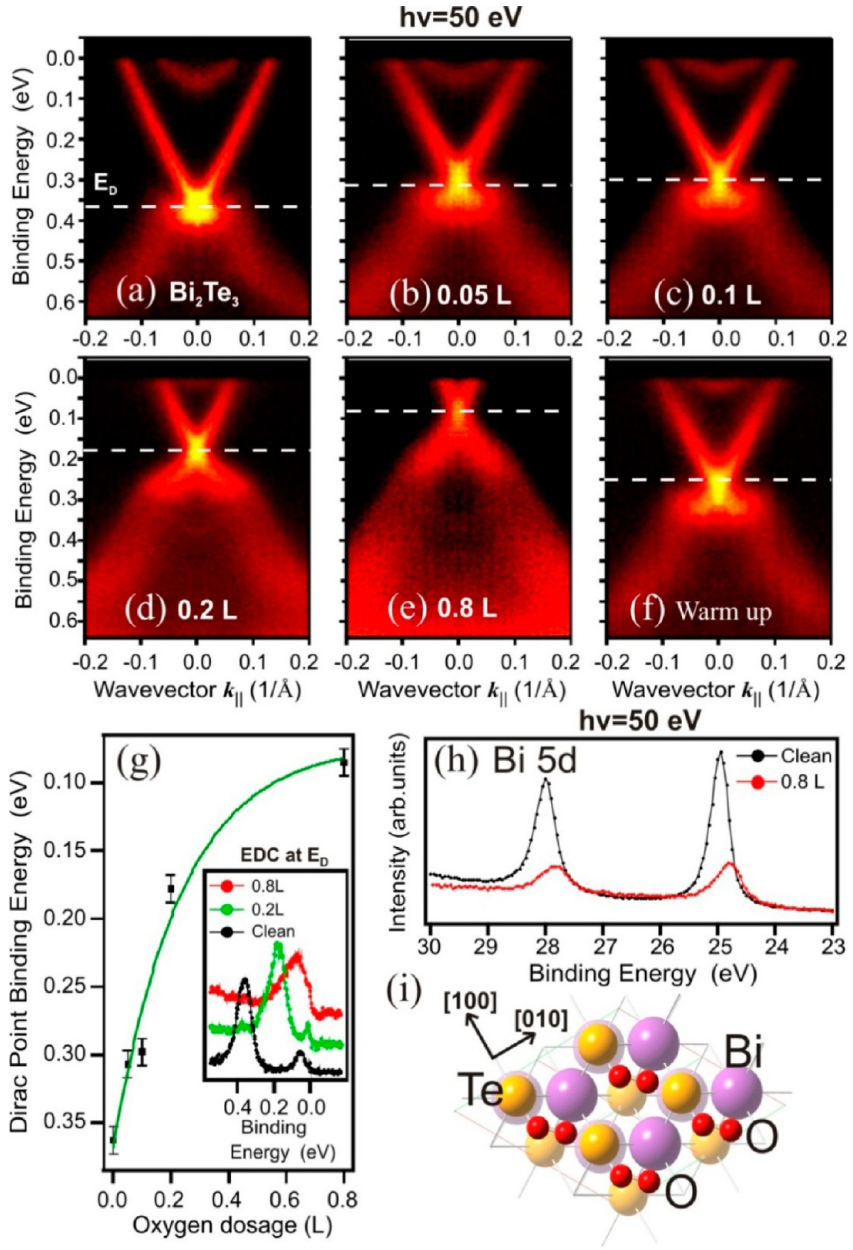

Figure 1. Oxygen exposure of Bi_2Te_3. High-resolution ARPES *E*(k) dispersions of the topological surface state measured for the Bi_2Te_3 crystals at 50 eV photon energy. (a–e) The influence of oxygen exposure at 30 K (the binding energy is calculated from Fermi level). Due to modification of the surface potential upon oxygen adsorption, the Fermi level shifts to higher binding energy. (f) Warming up to room temperature reverses the effect. (g) Binding energy dependence of the Dirac point on oxygen dosage. Inset: the corresponding energy dispersion curves (EDCs) extracted at zero momentum. (h) The Bi 5d core levels before and after 0.8 L oxygen exposure. (i) DFT modeling results showing the optimized Bi_2Te_3 structure with the most stable position of oxygen molecules on the surface.

cannot be confirmed on the basis of our ARPES data. Besides, we cannot reproduce the donor doping effect observed in ref 14, but observe rather weak acceptor doping. We emphasize that our DFT calculations also predict a weak acceptor doping effect (Fermi level shift by 0.10 eV) for the H_2O/Bi_2Te_3 system (see Table 1). The difference of our results with previously reported data[14,28] could be assigned to the different initial defect concentration, which is higher in our case. Despite of the fact that we have reproduced exactly the sample conditioning of ref 14, it should be noted that the water adsorption is less pronounced than the one for oxygen. This can be concluded from the comparison of the core level spectra before and after adsorption (see Figures 1h, 2f,g). At low coverage the position of water molecules at the surface may be different; and different adsorption structures result in different doping levels as it follows from our calculated data.

For device applications, however, the influence of near-ambient vapor pressures on the surface states is of great interest. Under such circumstances, high-pressure XPS represents a powerful tool to study the

TABLE 1. The Summary of Modeling Results for O_2, H_2O Physical Adsorption on Bi_2X_3 (111) Surfaces (X = Se,Te)

Structure	Relative adsorption energy of isomers*, eV	Fermi level shift calculated relative to bulk Bi_2X_3, eV
Bi_2Se_3+O_2		
hollow position, O-O is nearly parallel to the surface	0	-0.13
Se on-top position, O-O is perpendicular to the surface	0.07	-0.46
Bi_2Se_3+H_2O		
water molecule at hollow site	0	-0.19
water molecule on-top of Se atom	0.03	-0.26
Bi_2Te_3+O_2		
hollow position, O-O is nearly parallel to the surface	0	-0.09
Te on-top position, O-O is perpendicular to the surface	0.34	-0.41
Bi_2Te_3+H_2O		
water molecule at hollow site	0	0.04
water molecule on-top of Te atom	0.06	-0.03
*0 is assigned to the more stable of two isomeric structures		

surface properties,[29] which indeed can be rather different from those for surfaces in vacuum. For this reason, we performed an *in situ* high pressure XPS experiment at a partial water pressure of $P(H_2O) \sim 0.10$ mbar during a period of 10 h. The results are depicted in Figure 4.

Since water forms a surface layer and its thickness increases gradually with time, we monitor the H_2O/Bi_2Te_3 interface by enhancing the probing depth using high photon energies (up to 1400 eV) to excite photoelectrons with kinetic energies up to 800 eV. Figure 4d shows the results obtained by calculating the water adsorption curve using the Hill equation (see Supporting Information). In general, the experiment was continued until the adsorbed water layer was as thick as ~4 nm. However, no modification of the Bi 4f and Te 3d core levels was observed even at this rather high water layer thickness limit. This means that the Bi_2Te_3 surface does not react with water. The O 1s peak can be treated as one broad component positioned at ~532.6 eV binding energy, which is assigned to water. Therefore, one can conclude that water does not react with the surface even at high water dosages up to 3.6×10^9 L. We emphasize that our DFT calculations also indicate that water does not dissociate at the surface. The water molecule, even when artificially decomposed into −H and −OH at the surface in our starting calculation geometry, is formed again as a structure which is energetically more favorable than a proton and a hydroxyl group bonded to the surface (see Table 1).

Moreover, one can conclude that the *in situ* experiments even at high pressure do not reveal the chemical changes at the surface of Bi_2Te_3 due to its very low reactivity at room temperature and the shortness of the exposure time as compared to the induction period, which is generally long due to the low probability of the elementary chemical reaction event.

When the surface is exposed to humid air, water and oxygen adsorb simultaneously in a proportion defined by the humidity. Our multiple *ex situ* experiments discussed below show that at any humidity the induction period for the surface reaction is at least about 8 h (which corresponds to dosages of $\sim 5 \times 10^{12}$ L O_2 and $\sim(1-5) \times 10^{11}$ L H_2O).

Surface Reaction and the Oxidation of the First Layer. We studied the surface reaction of Bi_2Te_3 *ex situ* after well-defined exposures to air at different relative humidities and to liquid water (both gas-free and not degassed). In the case of *ex situ* experiments at room temperature, physically adsorbed species are believed to desorb during evacuation in the spectrometer. To provide ultimate surface sensitivity and spectral resolution, Bi 5d and Te 4d spectra were recorded at 125 eV photon energy. We demonstrate below that the reaction mechanism and the induction period appear to be

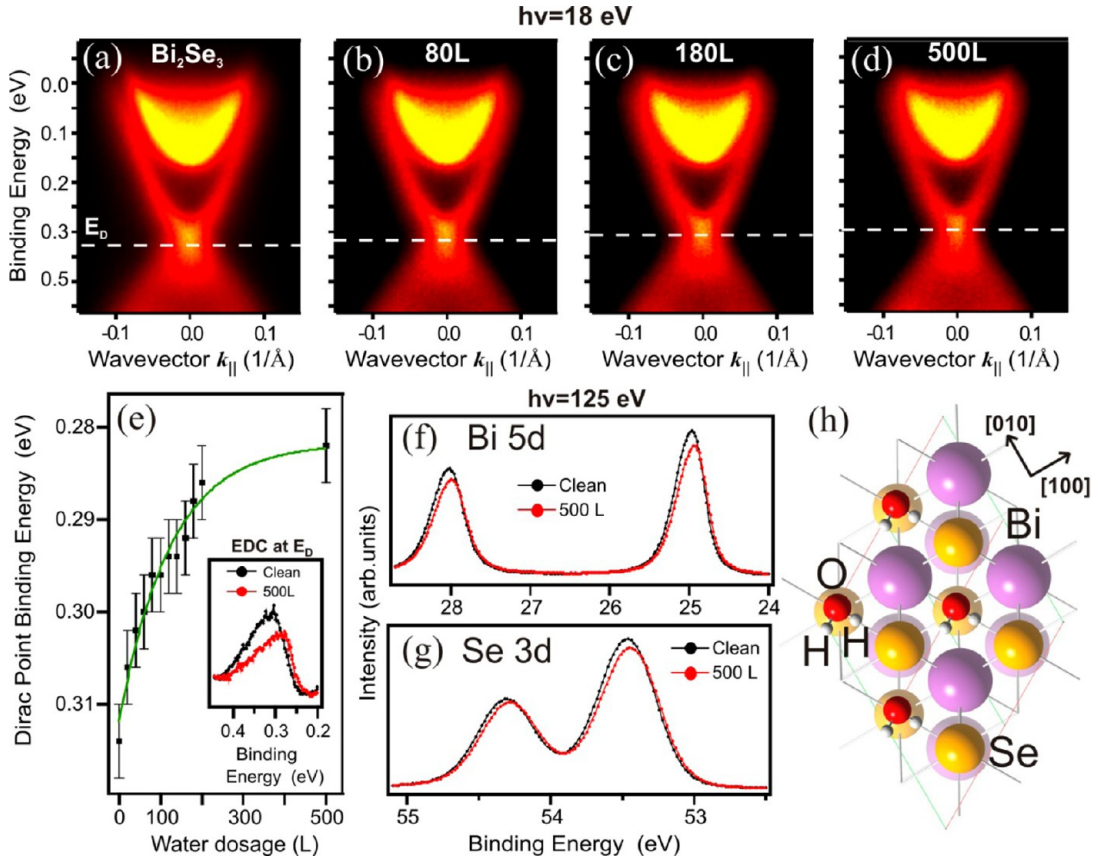

Figure 2. Water exposure of Bi_2Se_3. High-resolution ARPES *E*(k) dispersions of the topological surface state measured on Bi_2Se_3 thin films at 18 eV photon energy. (a–d) Influence of water exposure at room temperature. (e) Binding energy dependence of the Dirac point on water dosage. Inset: EDCs extracted at zero momentum. (f) Bi 5d and (g) Se 3d core levels before and after 500 L water exposure measured at 125 eV photon energy. (i) The DFT modeling results showing the optimized Bi_2Se_3 structure with the most stable configuration of the water molecules on the surface.

different for high and low relative humidities. Oxidation in dry air is rather slow as compared to that at a relatively low humidity of 10%, as described further below. We anticipate first that water vapor must play a key role in the surface oxidation and second that the surface reaction is possible in the simultaneous presence of both water and oxygen. The corresponding data are presented in Figures 5 and 6.

At high humidity as well as in liquid water, the surface product formed at the beginning of the process is the same. It includes a slightly oxidized tellurium with a chemical shift of +1.3 eV (corresponding to Te^0) and reduced Bi atoms with a chemical shift of −1.0 eV (corresponding to Bi^{+2}) after 1 day of exposure, *i.e.*, $\sim 10^{14}$ L (Table 2). The O 1s peak is observed at a binding energy of 531.5 eV, which differs from the value of 532.6 eV observed for water during the *in situ* studies, as discussed above. The peak positioned at 531.5 eV may be assigned to surface hydroxyl groups, since under UHV conditions molecular water desorbs. Based on the comparison of experimentally observed chemical shifts with the DFT-calculated ones, the surface reaction results in two hydroxyl groups bonded to neighboring tellurium atoms (see Figure 7a). This stable structure is formed in the presence of both oxygen and water due to the following reaction:

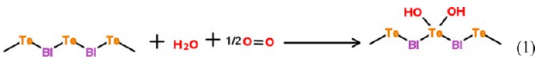

Equation 1 describes the first stage of oxidation in air.

Further oxidation, when the surface is fully terminated by the −OH groups, results in the appearance of new components in both Te 4d and Bi 5d spectra. The component shifted by +3.80 eV in the Te 5d spectrum corresponds to the formal oxidation state +4;[22,30] this situation corresponds to the Bi−O−Te bond formation. In the Bi 5d spectrum, the feature split by +1.38 eV from the initial peak corresponds to the formation of more ionic Bi−O bonds in the Bi−O−Te fragment with the same formal Bi oxidation state (+3). In the O 1s spectra, a component positioned at 529.6 eV appears, which corresponds to the formation of oxide-type bonds. The corresponding optimized structure is presented in Figure 7b.

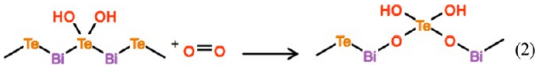

It should be noted that at 84% humidity the transformation from stage (1) to stage (2) takes place

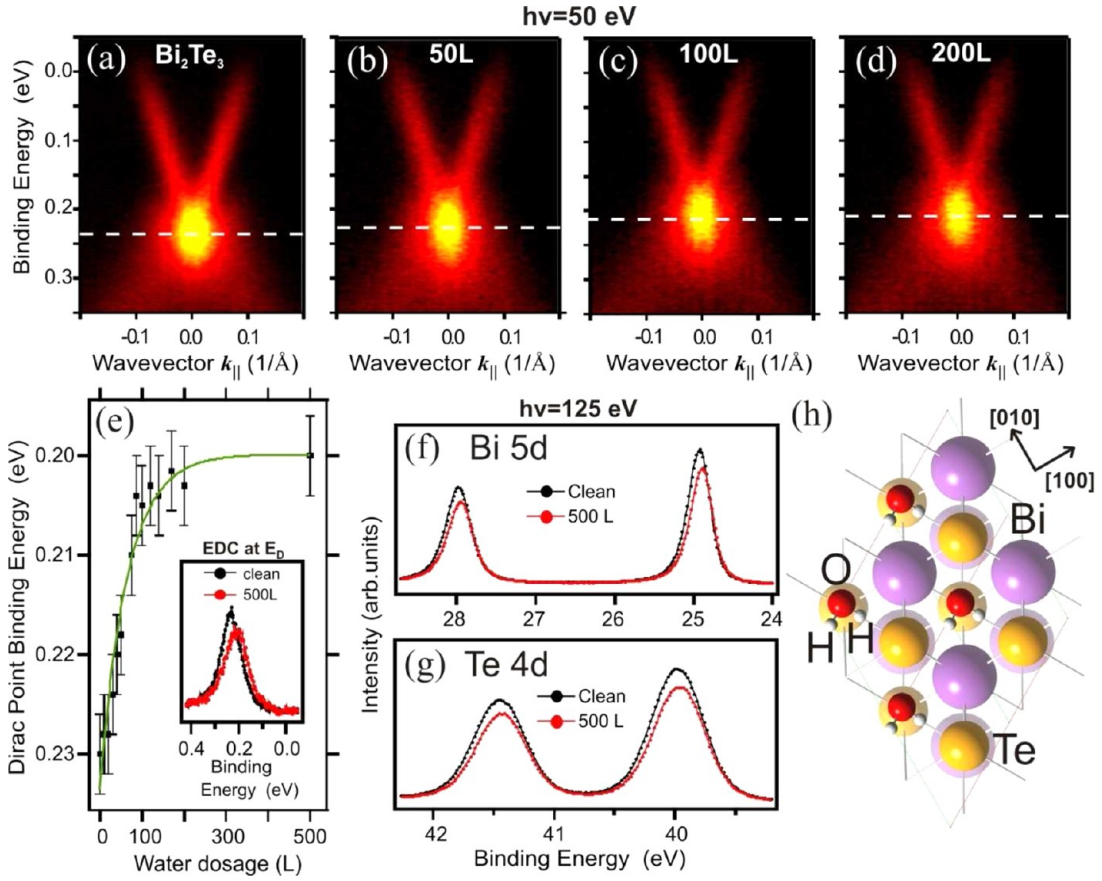

Figure 3. Water exposure of Bi_2Te_3. Similar data as in Figure 2 measured for the Bi_2Te_3 crystals at 50 eV photon energy. (a–d) The influence of water exposure at room temperature. (e) Binding energy dependence of the Dirac point on water dosage up to saturation. Inset: EDCs extracted at zero momentum. (f–g) Bi 5d and Te3d core levels before and after 500 L water exposure. (h) The DFT modeling results show the optimized Bi_2Te_3 structure revealing the most stable position of the water molecules on the surface.

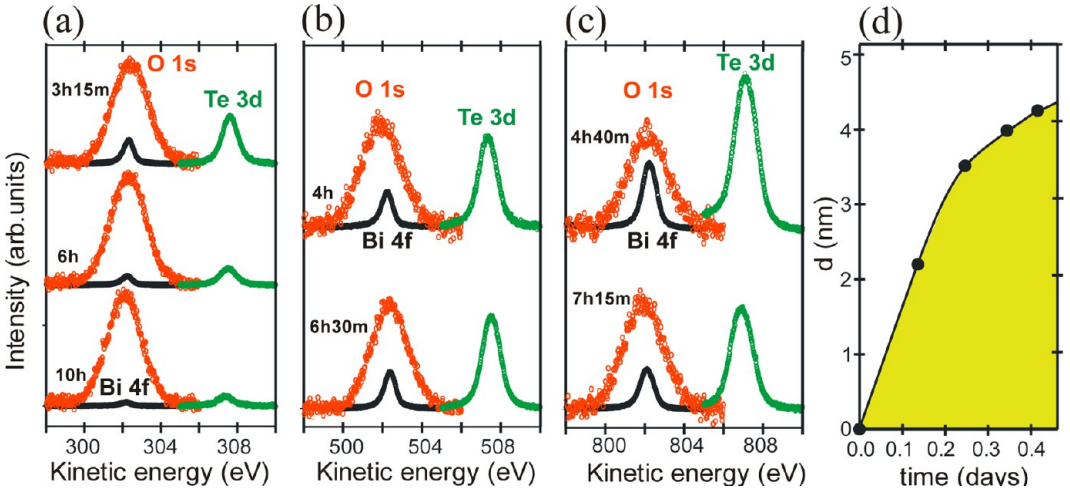

Figure 4. Water exposure of Bi_2Te_3. Core level spectra for the Bi_2Te_3(111) surface exposed *in situ* to 0.1 mbar H_2O and recorded at different exposure times and kinetic energies of (a) 300 eV, (b) 500 eV, and (c) 800 eV corresponding to the increasing probing depth. (d) Time dependence of the water layer thickness calculated using the Hill equation (see Supporting Information).

after about 1 day of exposure, as it is clearly seen in Figure 5b. The surface layer is fully oxidized after about 30 h.

The results obtained for liquid water containing dissolved air are similar to those at 84% humidity. In degassed water, on the other hand, the reaction is noticeably slower as follows from the spectra presented in Figure 6.

At a moderate humidity of 44%, which is close to ambient conditions, the reaction starts earlier (after 8 h, *i.e.*, 2×10^{13} L), and the first stage of oxidation is not pronounced and generally slower (see Figures 4a–c).

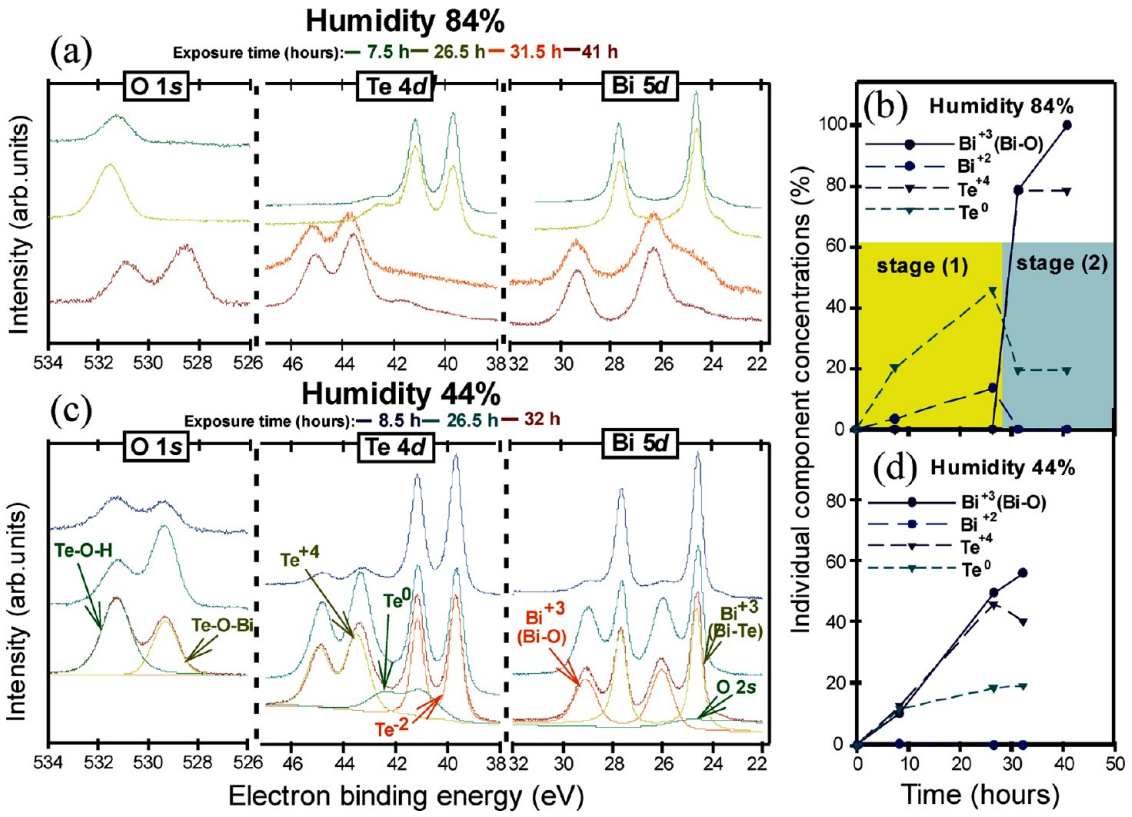

Figure 5. Air exposure of Bi_2Te_3. Series of the O 1s, Te 4d, Bi 5d core level spectra for different time points of the Bi_2Te_3 (111) air oxidation obtained at 125 eV photon energy after oxidation in air at 23 ± 2 °C and 84% humidity (a) and 44% humidity (c) and the corresponding intensity variation of the individual spectral features with time (b and d).

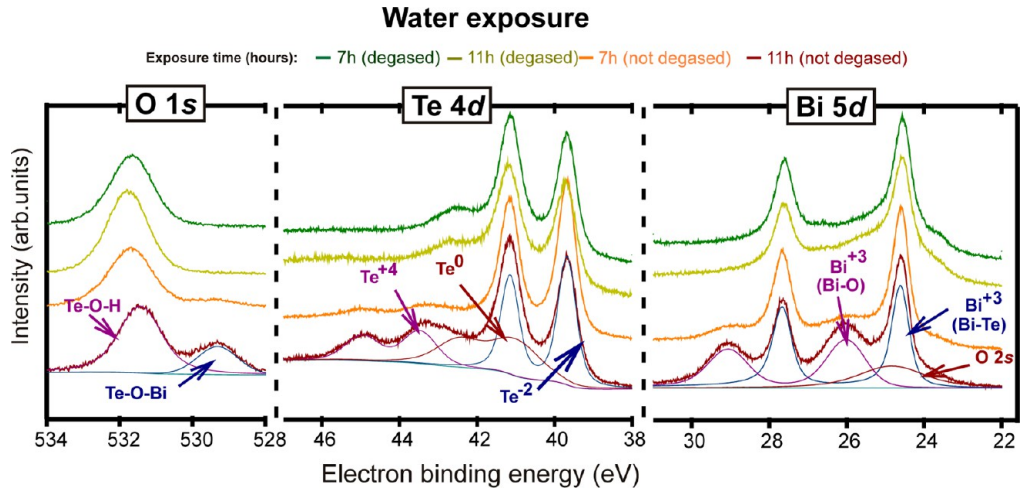

Figure 6. Water exposure of Bi_2Te_3. Series of the O 1s, Te 4d, Bi 5d core level spectra for Bi_2Te_3 (111) surface after its oxidation in degassed and nondegassed water at 23 ± 2 °C at two time points for 7 and 11 h obtained at 125 eV photon energy.

The intensities of the Bi−O, Te^0 and Te^{+4} components gradually increase with the exposure time. In the O 1s spectra there are two components assigned to hydroxide and oxide structures. We checked the variation of relative intensity ratios for different spectral components with the detection angle and hence surface sensitivity (see Supporting Information). The results indicate that the Te^0 and hydroxyl−oxygen bonds are always closer to the surface corresponding to the formation of the surface Te−OH groups.

The difference in the oxidation behavior at high and moderate humidity can be explained by the formation of a water layer at the surface, which partially blocks the reaction with oxygen. This results in a lower oxidation rate during stage (1) at higher humidity and in liquid water. It should be noted that we would expect one more air constituent, CO_2, to play an essential role in the surface degradation. However, we have never observed carbonate-related species on the air-exposed surfaces in our experiments. Therefore, we

TABLE 2. The Summary of Modeling Results for O_2+H_2O Chemisorption on Bi_2Te_3 (111)

Structure	Calculated Te 4*d* shift, eV	Calculated Bi 5*d* shift, eV	Experimental Te 4*d* shift, eV	Experimental Bi 5*d* shift, eV
Bi_2Te_3OH	0.50	-0.31		
$Bi_2Te_3(OH)_2$	0.95	-0.75	1.3	-1
$Bi_2Te_3(OH)_3$	1.89	-0.85		
$Bi_2Te_3(OH)_2O$	1.00	-0.17		
$Bi_2Te_3(OH)_2O_2$	2.37	0.48		
$Bi_2Te_3(OH)_2O_3$	2.97	1.11	3.8	1.38

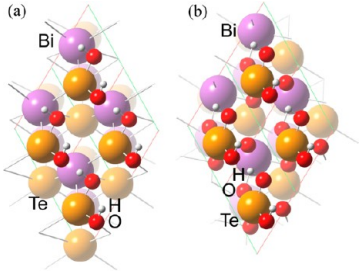

Figure 7. Optimized atomic geometry for structures Bi_2Te_3-$(OH)_2$ (a) and $Bi_2Te_3(OH)_2O_3$ (b).

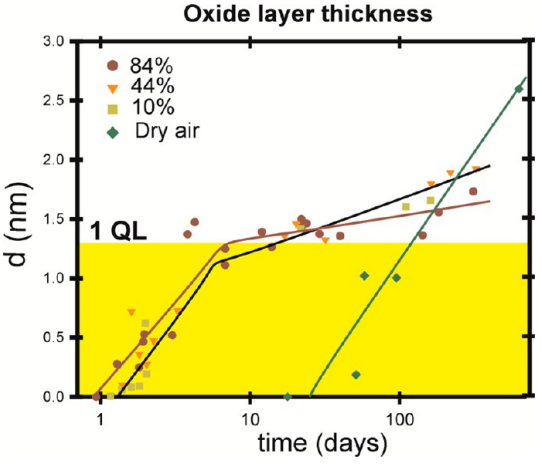

Figure 8. Air exposure of Bi_2Te_3. The oxidation kinetics for the Bi_2Te_3(111) surface at 23 ± 2 °C: time dependence of the oxide layer thickness for oxidation in dry and wet air at humidities of 10, 44 and 84%. The initial spectra were obtained using a monochromatic Al $K_\alpha$source.

may conclude that CO_2 plays no role in the surface degradation.

It should be noted that the same conditioning was applied to Bi_2Se_3 as well. However, we found no changes in core level spectra taken at ultimately high surface sensitivity.

In-Depth Oxidation with Long-Term Kinetics. The oxidation kinetics for Bi_2Te_3, *i.e.*, the time-dependent variation of the oxide layer thickness calculated from core level data using the Hill equation, is presented in Figure 8 for dry and humid air, correspondingly. One can see that the oxidation in dry air is very slow (this may be caused by a residual humidity because the presence of residual water is unavoidable). The main reason for the scattering of the experimental points for each humidity value is probably related to the statistical nature of the chemical reaction event at relatively high induction periods (each point corresponds to an individual sample). Nevertheless, the estimated standard error, which includes effects from the surface nonuniformity, weak time-dependent UHV effects and the reproducibility of the fit procedure, does not exceed 0.05 nm. Generally, within the complete oxidation period, the resulting reaction products are very similar: they are revealed in the spectra of Figures 5 and 6 as distinct Bi−O and Te^{+4} spectral components and at low exposures as Te^0-related features. Moreover, the O 1s spectra have a two-component structure: one of these components corresponds to the surface hydroxyl groups and the other one is of oxide nature. In particular, the oxide layer composition corresponds to the formal stoichiometry of $Bi_2Te_3O_7(OH)_4$. We emphasize that multiple small spot analysis of the chemical composition carried out for each exposure time revealed a very high uniformity of the oxide layer within a lateral scale of 1−100 μm (not shown here).

At a relatively high humidity of 84%, the oxidation rate is somewhat higher at the beginning of the process, and it becomes lower after the oxidation of one quintuple layer (QL) after 5 days (~10^{14} L) (1 QL~ 1 nm). We emphasize that this difference between various humidities is not related to the oxide layer morphology. We have performed AFM studies of clean and oxidized surfaces exposed for periods of time longer than 100 days and did not observe any changes in the surface morphology within a typical noise level of 0.1 nm (not shown here). We typically observed a very low density of steps corresponding to the thickness variations within 1 QL/μm^2, meaning that the oxide layer is relatively flat and uniform. Besides, there are no differences between the surfaces oxidized at different humidities. Most probably, this is related to the fact that at high humidity water forms a layer at the surface which prevents further oxidation due to limited diffusion. On the other hand, in the middle range of humidities

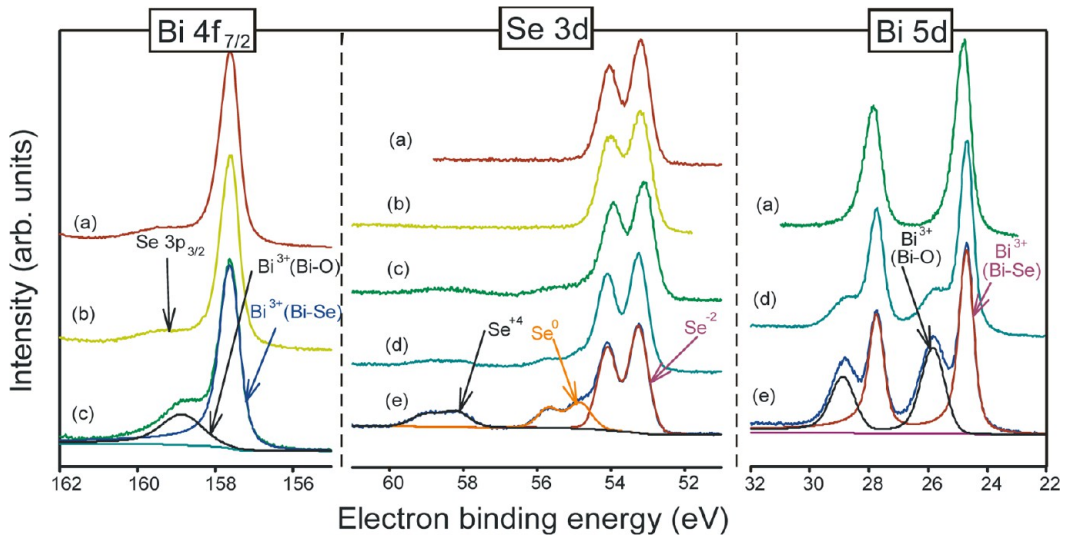

Figure 9. Bi $4f_{7/2}$ (left), Se 3d (center) and Bi 5d (right) core level photoemission spectra of Bi_2Se_3 (111) surface of single crystal and epitaxial film exposed to dry and humid air and for long periods of time: (a) clean surface of a crystal; (b) oxidized surface of a crystal after 259 days in dry air; (c) oxidized surface of a crystal after 378 days at 84% humidity; (d) oxidized surface of MBE film after 30 days at 44% humidity; (e) oxidized surface of MBE film after 140 days at 44% humidity.

our results indicate that the oxidation kinetics does not depend strongly on the humidity. At the humidities of 10% and 44%, the oxidation kinetics of 1 QL is slower. The oxide thickness is in reasonable agreement with the previous observations for humidities of ~30%.[22]

Finally, regarding the oxidation kinetics of Bi_2Se_3 crystal, we emphasize that we only observe pronounced doping effects in the ARPES dispersions during stage (i) corresponding to molecular absorption, but no changes in the Bi and Se core level photoemission spectra during stage (ii) were observed, as discussed above. Furthermore, considering that no reaction occurs even after 2 years in dry air and up to 1 year at 84% humidity, we conclude that the surface of Bi_2Se_3 bulk crystal does not undergo surface oxidation in dry air or air of moderate humidity within a wide time range. It should be noted that after more than 1 year at 84% humidity we observed minor surface oxidation of the Bi_2Se_3 surface, which is in line with negligible surface reactivity of bismuth selenide. The corresponding spectra are shown in Figure 9. It should be noted that MBE-grown epilayers exhibit higher reactivity; the noticeable oxidation is seen after one month of air exposure. Taking into account literature data on fast oxidation of nanoribbon[25] and the behavior of a sputtered bulk crystal surface, *i.e.* mixing layer,[27] one can suppose that the difference in reactivity between a cleaved surface of a bulk crystal and a MBE-grown epilayer is probably related to a different surface structure and termination resulting from the different surface preparation procedures.

CONCLUSIONS

In summary, our systematic photoemission studies in a wide range of experimental conditions, as well as the DFT calculations, show that both O_2 and H_2O adsorb molecularly at the Bi_2Te_3 and Bi_2Se_3 surfaces. Only simultaneous adsorption of water and oxygen after prolonged exposure (~5×10^{12} L O_2) results in a surface reaction in the case of Bi_2Te_3. This reaction includes two steps: (1) surface termination with hydroxyl groups attached to the Te atoms, and (2) formation of oxide species with oxygen bonded to both Bi and Te atoms. For humid air, there is continuous oxidation with the inflection point corresponding to the oxidation of 1 QL (~10^{14} L). Thus, the time scale for oxidation in wet air is well understood for Bi_2Te_3. For Bi_2Se_3 crystals, we have observed high stability against oxidation; the surfaces do not react even after 2 years in dry air and up to 1 year at 84% relative humidity. Bi_2Se_3 films are evidently more reactive. Nevertheless, compared to bismuth telluride, Bi_2Se_3 is much more inert; therefore, it is more favorable for applications. Negligible surface reactivity is important for topological insulator based applications. Our results provide important implications regarding the acceptable ranges of conditions for preparation, handling and operation of the future Bi_2Te_3- and Bi_2Se_3-based devices. Moreover, the absence of any chemical transformations and presumably physical adsorption makes these surfaces useful for resistivity-based sensors.

METHODS

Bi_2Se_3 and Bi_2Te_3 n-type single crystals and thin films were grown by the Bridgman method and by molecular beam epitaxy (MBE) on BaF_2 (111), respectively. Both films and bulk crystals have approximately the same doping level. Bulk single crystals were cleaved *in situ* for ARPES and near ambient pressure (NAP) XPS experiments or *ex situ* for the photoemission studies of oxidation at high exposures. The 400 nm thick MBE

films were grown using Bi_2Se_3 and Se, or Bi_2Te_3 and Te source materials, respectively. The temperature of the BaF_2 substrate was 360 °C, which led to two-dimensional growth observed by *in situ* reflection high-energy electron diffraction. The epilayers were capped by a 50 nm thick amorphous Se layer after cooling to room temperature in order to protect them during transport in air . The cap layer was removed inside of the photoemission setup by annealing at ≈230 °C for ≈1 h. The high quality of the achieved (111) surfaces was verified by low-energy electron diffraction (LEED), the presence of sharp features from the topological surface states and the valence band in the ARPES dispersions.

Photoemission studies were carried out using several facilities of Helmholtz-Zentrum Berlin, Germany. The *in situ* ARPES experiments were carried out in ultrahigh vacuum better than 10^{-10} mbar and at oxygen or water partial pressure of 10^{-6} mbar with a Scienta R8000 electron analyzer at the UE112-PGM2a beamline using p-polarized undulator radiation. The NAP XPS data were obtained at the ISISS beamline equipped with a SPECS Phoibos 150 analyzer under water pressures of ~0.1 mbar. The Bi 4f, Te 3d and O 1s spectra were recorded at different kinetic energies between 200 and 800 eV to provide variable surface sensitivity.

For *ex situ* experiments, freshly cleaved surfaces were exposed for defined periods of time to dried or humid air at 1 bar and 23 ± 2 °C. The Bi 5d, Te 4d and O 1s spectra were recorded with high surface sensitivity at the Russian–German beamline (the photon energy was 125 eV for Bi 5d and Te 4d and 600 eV for the O 1s core levels). The XPS spectra acquisition was performed using a SPECS Phoibos 150 electron energy analyzer at variable detection angles.

The long-term oxidation kinetics was studied using a Kratos Axis Ultra laboratory system equipped with a monochromatic Al K_α X-ray source. All XPS spectra were fitted by Gaussian/Lorentzian convolution functions with simultaneous optimization of the background parameters. The line asymmetry of high resolution Bi 5d core level was described with Doniach–Sŭnjić functions. The background was modeled using a combination of Shirley and Tougaard backgrounds.

Theoretical modeling of the surface reactions was performed within the DFT approach using the PW-GGA method (VASP code).[31−33] A single quintuple layer was considered. In all cases listed below ($7 \times 7 \times 1$) *k*-points mesh of first Brillouin zone was used. A ($5 \times 5 \times 1$) *k*-points mesh gives data scattering of 0.01–0.07 eV. No superlattice was used. Lattice constants were fixed, while positions of all atoms were varied. Core level shifts were calculated in the initial state approximation as the variation of electrostatic potentials at atomic centers after adsorption as described in ref 30.

Conflict of Interest: The authors declare no competing financial interest.

Supporting Information Available: Calculation of water layer thickness in the *in situ* experiments, angular dependent core level spectra of the oxidized Bi_2Te_3 (111) surface. This material is available free of charge *via* the Internet at http://pubs.acs.org.

Acknowledgment. The authors acknowledge the financial support within the bilateral Program, "Russian-German Laboratory at BESSY II" and would like to thank Helmholtz-Zentrum Berlin for granting access to UE112-PGM2a beamline and Fritz-Haber-Institut Berlin/HZB for access to ISISS beamline. The DFT calculations were performed using SKIF MSU "Lomonosov" supercomputer, Supercomputing Center of Lomonosov Moscow State University. V. S. Neudachina acknowledges the support of the G-RISC Centre of Excellence. The work was partially supported by Helmholtz Gemeinschaft and RFBR (grant 13-02-91327).

REFERENCES AND NOTES

1. Kane, C. L.; Mele, E. J. Z_2 Topological Order and the Quantum Spin Hall Effect. *Phys. Rev. Lett.* **2005**, *95*, 146802.
2. Kane, C. L.; Mele, E. J. Quantum Spin Hall Effect in Graphene. *Phys. Rev. Lett.* **2005**, *95*, 226801.
3. Fu, L.; Kane, C. L. Topological Insulators with Inversion Symmetry. *Phys. Rev. B* **2007**, *76*, 045302.
4. Bernevig, B. A.; Zhang, S. C. Quantum Spin Hall Effect. *Phys. Rev. Lett.* **2006**, *96*, 106802.
5. Fu, L.; Kane, C. L.; Mele, E. J. Topological Insulators in Three Dimensions. *Phys. Rev. Lett.* **2007**, *98*, 106803.
6. Moore, J. E.; Balents, L. Topological Invariants of Time-Reversal-Invariant Band Structures. *Phys. Rev. B* **2007**, *75*, 121306(R).
7. Roy, R. Topological Phases and the Quantum Spin Hall Effect in Three Dimensions. *Phys. Rev. B* **2009**, *79*, 195322.
8. Murakami, S. Phase Transition between the Quantum Spin Hall and Insulator Phases in 3D: Emergence of a Topological Gapless Phase. *New J. Phys.* **2007**, *9*, 356.
9. Castro Neto, A. H.; Guinea, F.; Peres, N. M. R.; Novoselov, K. S.; Geim, A. K. The Electronic Properties of Graphene. *Rev. Mod. Phys.* **2009**, *81*, 109–162.
10. Hsieh, D.; Xia, Y.; Wray, L.; Qian, D.; Pal, A.; Dil, J. H.; Osterwalder, J.; Meier, F.; Bihlmayer, G.; Kane, C. L.; *et al.* Observation of Unconventional Quantum Spin Textures in Topological Insulators. *Science* **2009**, *323*, 919–922.
11. Hasan, M. Z.; Kane, C. L. Colloquium: Topological Insulators. *Rev. Mod. Phys.* **2010**, *82*, 3045–3067.
12. Plucinski, L.; Mussler, G.; Krumrain, J.; Herdt, A.; Suga, S.; Grützmacher, D.; Schneider, C. M. Robust Surface Electronic Properties of Topological Insulators: Bi_2Te_3 Films Grown by Molecular Beam Epitaxy. *Appl. Phys. Lett.* **2011**, *98*, 222503.
13. King, P. D. C.; Hatch, R. C.; Bianchi, M.; Ovsyannikov, R.; Lupulescu, C.; Landolt, G.; Slomski, B.; Dil, J. H.; Guan, D.; Mi, J. L.; *et al.* Large Tunable Rashba Spin Splitting of a Two-Dimensional Electron Gas in Bi_2Se_3. *Phys. Rev. Lett.* **2011**, *107*, 096802.
14. Benia, H. M.; Lin, C.; Kern, K.; Ast, C. R. Reactive Chemical Doping of the Bi_2Se_3 Topological Insulator. *Phys. Rev. Lett.* **2011**, *107*, 177602.
15. Hirahara, T.; Bihlmayer, G.; Sakamoto, Y.; Yamada, M.; Miyazaki, H.; Kimura, S.-I.; Blügel, S.; Hasegawa, S. Interfacing 2D and 3D Topological Insulators: Bi(111) Bilayer on Bi_2Te_3. *Phys. Rev. Lett.* **2011**, *107*, 166801.
16. Bianchi, M.; Hatch, R. C.; Mi, J.; Iversen, B. B. Hofmann, Ph. Simultaneous Quantization of Bulk Conduction and Valence States through Adsorption of Nonmagnetic Impurities on Bi_2Se_3. *Phys. Rev. Lett.* **2011**, *107*, 086802.
17. Valla, T.; Pan, Z.-H.; Gardner, D.; Lee, Y. S.; Chu, S. Photoemission Spectroscopy of Magnetic and Nonmagnetic Impurities on the Surface of the Bi_2Se_3 Topological Insulator. *Phys. Rev. Lett.* **2012**, *108*, 117601.
18. Scholz, M. R.; Sánchez-Barriga, J.; Marchenko, D.; Varykhalov, A.; Volykhov, A.; Yashina, L. V.; Rader, O. Tolerance of Topological Surface States towards Magnetic Moments: Fe on Bi_2Se_3. *Phys. Rev. Lett.* **2012**, *108*, 256810.
19. Drapak, S. I.; Gavrylyuk, S. V.; Kovalyuk, Z. D.; Lytvyn, O. S. Age-Induced Oxide on Cleaved Surface of Layered GaSe Single Crystals. *Appl. Surf. Sci.* **2008**, *254*, 2067–2071.
20. Yashina, L. V.; Püttner, R.; Volykhov, A. A.; Stojanov, P.; Riley, J.; Vassiliev, S. Yu.; Chaika, A. N.; Dedyulin, S. N.; Tamm, M. E.; Vyalikh, D. V.; *et al.* Atomic Geometry and Electron Structure of the GaTe (10–2) Surface. *Phys. Rev. B* **2012**, *85*, 075409.
21. Volykhov, A. A.; Yashina, L. V.; Zyubina, T. S.; Neudachina, V. S.; Püttner, R. Comparative Reactivity of $A^{IV}B^{VI}$ Compounds in Their Reactions with Dioxygen. *Russ. J. Inorg. Chem.* **2011**, *56*, 1284–1289.
22. Bando, H.; Koizumi, K.; Oikawa, Y.; Daikohara, K.; Kulbachinskii, V. A.; Ozaki, H. The Time-Dependent Process of Oxidation of the Surface of Bi_2Te_3 Studied by X-ray Photoelectron Spectroscopy. *J. Phys.: Condens. Matter* **2000**, *12*, 5607–5616.
23. Chen, Y. L.; Chu, J. -H.; Analytis, J. G.; Liu, Z. K.; Igarashi, K.; Kuo, H. -H.; Qi, X. L.; Mo, S. K.; Moore, R. G.; Lu, D. H.; *et al.* Massive Dirac Fermion on the Surface of a Magnetically Doped Topological Insulator. *Science* **2010**, *329*, 659–662.
24. Wang, X.; Bian, G.; Miller, T.; Chiang, T.-C. Fragility of Surface States and Robustness of Topological Order in Bi_2Se_3 against Oxidation. *Phys. Rev. Lett.* **2012**, *108*, 096404.

25. Kong, D. S.; Cha, J. J.; Lai, K. J.; Peng, H. L.; Analytis, J. G.; Meister, S.; Chen, Y. L.; Zhang, H. J.; Fisher, I. R.; Shen, Z. X.; *et al.* Rapid Surface Oxidation as a Source of Surface Degradation Factor for Bi_2Se_3. *ACS Nano* **2011**, *5*, 4698–4703.
26. Atuchin, V. V.; Golyashov, V. A.; Kokh, K. A.; Korolkov, I. V.; Kozhukhov, A. S.; Kruchinin, V. N.; Makarenko, S. V.; Pokrovsky, L. D.; Prosvirin, I. P.; Romanyuk, K. N.; *et al.* Formation of Inert Bi_2Se_3 (0001) Cleaved Surface. *Cryst. Growth Des.* **2011**, *11*, 5507–5514.
27. Golyashov, V. A.; Kokh, K. A.; Makarenko, S. V.; Romanyuk, K. N.; Prosvirin, I. P.; Kalinkin, A. V.; Tereshchenko, O. E.; Kozhukhov, A. S.; Sheglov, D. V.; Eremeev, S. V.; *et al.* Inertness and Degradation of (0001) Surface of Bi_2Se_3 Topological Insulator. *J. Appl. Phys.* **2012**, *112*, 113702.
28. Analytis, J. G; Chu, J.-H.; Chen, Y.; Corredor, F.; McDonald, R. D.; Shen, Z. X.; Fisher, I. R. Bulk Fermi Surface Coexistence with Dirac Surface State in Bi_2Se_3: A Comparison of Photoemissionand Shubnikov−de Haas Measurements. *Phys. Rev. B.* **2010**, *81*, 205407.
29. Salmerón, M.; Schlogl, R. Ambient Pressure Photoelectron Spectroscopy: A New Tool for Surface Science and Nanotechnology. *Surf. Sci. Rep.* **2008**, *63*, 169–199.
30. Yashina, L. V.; Zyubina, T. S.; Püttner, R.; Zyubin, A. S.; Shtanov, V. I.; Tikhonov, E. V. A Combined Photoelectron Spectroscopy and *ab Initio* Study of the Adsorbate System O_2/PbTe(001) and the Oxide Layer Growth Kinetics. *J. Phys. Chem. C* **2008**, *112*, 19995–20006.
31. Kresse, G.; Hafner, J. *Ab Initio* Molecular Dynamics for Liquid Metals. *Phys. Rev. B* **1993**, *47*, 558.
32. Kresse, G.; Hafner, J. *Ab Initio* Molecular Dynamics for Open-Shell Transition Metals. *Phys. Rev. B* **1993**, *48*, 13115–13118.
33. Kresse, G.; Hafner, J. *Ab Initio* Molecular-Dynamics Simulation of the Liquid-Metal−Amorphous-Semiconductor Transition in Germanium. *Phys. Rev. B* **1994**, *49*, 14251–14269.